Journal of Sensor Science and Technology
Vol. 32, No. 3 (2023) pp. 147-153
http://dx.doi.org/10.46670/JSST.2023.32.3.147
pISSN 1225-5475/eISSN 2093-7563

Quantitative Analysis of SO_2 and NO_2 Adsorption and Desorption on Quartz Crystal Microbalance Coated with Cobalt Gallate Metal-Organic Framework

Junhyuck Ahn[1], Taewook Kim[1,2], Sunghwan Park[1,2], Young-Sei Lee[1,2,+], and Changyong Yim[1,2,+]

Abstract

Metal-organic frameworks (MOFs) of cobalt gallate were synthesized and deposited on gold electrodes using self-assembly monolayers (SAMs) and hydrothermal processing. These MOF films exhibit strong adsorption capabilities for gaseous particulates, and the use of SAMs allows the synthesis and deposition processes to be completed in a single step. When cobalt gallate is mixed with SAMs, a coordination bond is formed between the cobalt ion and the carboxylate or hydroxyl groups of the SAMs, particularly under hydrothermal conditions. Additionally, the quartz crystal microbalance (QCM) gas sensor accurately measures the number of particulates adsorbed on the MOF films in real-time. Thus, the QCM gas sensor is a valuable tool for quantitatively measuring gases, such as SO_2, NO_2, and CO_2. Furthermore, the QCM MOF film gas sensor was more effective for gas adsorption than the MOF particles alone and allowed the accurate modeling of gas adsorption. Moreover, the QCM MOF films accurately detect the adsorption-desorption mechanisms of SO_2 and NO_2, which exist as gaseous particulate matter, at specific gas concentrations.

Keywords: Metal-organic framework, Quartz crystal microbalance, Gaseous particulate matter, Gas adsorption kinetics, Self-assembly monolayer

1. INTRODUCTION

Metal-organic frameworks (MOFs) and metal oxides are representative categories of gas-sensing materials [1-3]. MOFs are porous materials characterized by their composition of metal ions or clusters interconnected by organic ligands. These materials have recently garnered considerable interest owing to their distinct structures, exceptional surface areas, and adaptable pore sizes. Their potential applications span a diverse range of fields, such as gas storage, catalysis, separation, and drug delivery systems [4].

MOFs are promising materials for gas sensors owing to their large surface area and tunable pore size. These properties allow for the efficient adsorption and detection of specific gases, providing high selectivity. Moreover, MOFs can be tailored to target individual gases, thereby enhancing their versatility in gas-sensing applications [5].

The quartz crystal microbalance (QCM) technique has been widely used for the development of MOF-based gas sensors. The QCM operates by detecting changes in the frequency of quartz crystal resonators caused by adsorption on their surfaces [6]. Integrating MOFs with the QCM enables the accurate and sensitive detection of gases, such as NO_2 and SO_2. These gases are associated with particulate matter pollution. They are often referred to as secondary particulate-inducing gases owing to their ability to form particulate matter in the atmosphere, which contributes to poor air quality and poses health risks. Therefore, the detection of these gases is critical for air-quality monitoring, highlighting the need for sensitive and selective sensors [7-9].

The fabrication of thin, porous MOF films introduces new possibilities for their use in various applications, such as optical coatings, catalysts, and molecular recognition. The methods for preparing these films range from attaching crystals to surfaces after synthesis, to organizing them into monolayer-like metal oxide crystals to direct the growth of MOF-type materials on self-assembly layers (SAMs) [10].

This study investigated the gas-sensing properties of cobalt gallate MOF films for the detection of NO_2, SO_2, and CO_2 using SAMs and a highly sensitive QCM sensor. This study highlights the potential of MOFs and the QCM as gas sensor materials for

[1]Department of Advanced Science and Technology Convergence, Kyungpook National University (KNU), 2559 Gyeongsang-daero, Sangju-si, Gyeongsangbuk-do, 37224, Korea
[2]Department of Energy Chemical Engineering, Kyungpook National University (KNU), 2559 Gyeongsang-daero, Sangju-si, Gyeongsangbuk-do, 37224, Republic of Korea, Korea
[+]Corresponding author: ysl@knu.ac.kr,cy.yim@knu.ac.kr
(Received: May. 3, 2023, Revised: May. 17, 2023, Accepted: May. 22, 2023)

identifying these gases and their applicability in the development of MOF-based sensors with enhanced performance and selectivity for air-quality monitoring. Furthermore, this study provides insights into the adsorption mechanism of cobalt gallate, contributing to a better understanding of its gas-sensing properties.

2. EXPERIMENTAL

2.1 Chemical Reagents

Cobalt chloride hexahydrate ($CoCl_2 \cdot 6H_2O$, 98 %), gallic acid monohydrate (3, 4, 5-trihydroxybenzoic acid monohydrate, $C_7H_8O_6$, 99 %), 11-mercapto-1-undecanol ($C_{11}H_{24}OS$, 97 %, referred to as 11-OH), and 11-mercaptoundecanoic acid ($C_{11}H_{22}O_2S$, 95 %, referred to as 11-COOH) were purchased from Sigma-Aldrich Co. (USA). 1-dodecanethiol ($C_{12}H_{26}S$, 98 %, referred to as 12-CH_3) and 1-octanethiol ($C_8H_{18}S$, 98 %, referred to as 8-CH_3) were purchased from Alfa Aesar Co. (Germany). Potassium hydroxide (KOH, 95 %) was purchased from Samchun Chemicals Co. (Korea). All the chemicals used in this study were of analytical grade and used without further purification. High-purity gases, such as CO_2 (99.99 %), N_2 (99.99 %), and a mixture of SO_2 and NO_2 (500 ppm with N_2 balanced), were provided by Singin Gastech Co., Ltd. (Korea).

2.2 Preparation of SAMs-coated QCM Gold Surfaces.

First, thiol-bonded SAM was formed on the gold surfaces of the QCM, which was cleaned with corona charge treatment for 10 min (Electro-Technic Products, Inc., Chicago) prior to the attachment of the monolayer. Then, the cleaned gold surfaces of the QCM were immersed in 10 mL of a 50 mM ethanolic solution of the 4-type thiol compound (11-OH, 11-COOH, 12-CH_3, and 8-CH_3) for 30 min. The functionalized devices were then carefully washed with ethanol to prevent the contamination of the organic functional layers.

2.3 Preparation of Cobalt Gallate Film and Particle

Cobalt gallate [$Co(OH)_2(C_6H_2(OH)_3COO)$] was synthesized using a previously reported method [11]. Briefly, $CoCl_2$ (12 mmol) and gallic acid monohydrate (24 mmol) were added to 60 mL of an aqueous KOH solution (0.16 M for cobalt gallate) in separate beakers. The mixture was stirred continuously at ambient temperature and pressure for 30 min. Subsequently, the mixtures were subjected to sonication treatment for 30 min and then transferred to a Teflon-lined autoclave for the hydrothermal process for 24 h at 120 °C with the QCM treated with SAMs. After the hydrothermal reaction, the product was cooled to room temperature; then, it was collected and washed with ethanol and deionized water three times each. Subsequently, a cobalt gallate film coated on the QCM was obtained. The cobalt gallate particles remaining in the autoclave were collected by washing. This process involved centrifugation at 3000 rpm for 30 min, which was repeated five times with a mixture of ethanol and deionized water. Subsequently, the particles were dried under an ultrahigh vacuum at 100 °C for 24 h to collect pure cobalt gallate particles. Then, 100 μL of the cobalt gallate solution with a concentration of 1 mg/mL was poured onto the QCM using drop casting, which resulted in the formation of cobalt gallate particles on the QCM electrode. The cobalt gallate particles and film QCM samples were degassed under an ultrahigh vacuum at 100 °C for 24 h before being transferred to the QCM equipment for measurement.

2.4 Gas Sensing Measurements using QCM.

During the gas experiments with the QCM equipment, SO_2, NO_2, and CO_2 gases were utilized and regulated by a mass flow controller for accurate gas concentration control. The QCM mass measurements were obtained by applying the Sauerbrey equation (Equation (1)), which is commonly used to relate the observed frequency shifts to the deposited mass [12]:

$$\Delta m = -\frac{A\sqrt{\rho\mu}}{2f_0^2}\Delta f \quad (1)$$

where Δm is the change in mass, A is the active surface area of the resonator (0.4 cm^2), and ρ and μ are the density (2.648 g/cm^3) and shear modulus (2.947×10^{11} $g/cm \cdot s^2$) of quartz, respectively. The resonance frequency of the unloaded resonator, which is typically 5 MHz at room temperature for an AT-cut quartz crystal, is denoted as f_0, and Δf is the change in the resonance frequency. This equation demonstrates that the frequency shifts are directly proportional to the deposited mass, enabling the quantification of the amount of material deposited on the QCM surface.

2.5 Materials Characterizations

The X-ray diffraction (XRD) patterns of the samples were analyzed using a Panalytical X'Pert X-ray diffractometer (Empyrean, Malvern, UK) with a copper target and a wavelength

of 1.54 Å. The measurements were performed in the range of 5 °–50 ° with a step size of 0.01 °. The surface morphologies of the samples were examined using field-emission scanning electron microscopy (FESEM; Hitachi Regulus 8220 model, Tokyo, Japan). The contact angles of the gold surfaces were determined using SmartDrop (Femtofab Co., SmartDrop Standard, Korea), whereas the morphology of the cobalt gallate film coated on the gold surfaces was characterized using optical microscopy (Carl Zeiss Co., Axiolab 5, Germany). The surface areas of the samples were measured using nitrogen adsorption–desorption isotherms at 77 K. These measurements were performed using a Brunauer–Emmett–Teller (BET) instrument (QUADRASORB evo, Boyton Beach, USA). Prior to the measurements, the samples were degassed at 373 K for 24 h under ultrahigh vacuum.

3. RESULTS AND DISCUSSIONS

3.1 Cobalt Gallate Deposited on QCM

Several steps were followed to synthesize a cobalt gallate film on the QCM, as illustrated in Fig. 1. In the first step (Fig. 1a), the SAM was coated onto the QCM, creating a stable platform for the subsequent deposition of cobalt gallate. In the subsequent step (Fig. 1b), the SAM-modified QCMs were immersed in an autoclave filled with a mixture of a metal precursor and gallic acid in a specific ratio for hydrothermal synthesis. The binding between the metal precursor and the SAM molecule varies depending on the final functional group of the SAM molecule, resulting in different levels of cobalt gallate coating for different SAMs. After the hydrothermal synthesis, the cobalt-gallate-coated QCM electrodes were cleaned and subjected to vacuum oven treatment at 100 °C for a full day (Fig. 1c). Finally, the electrodes were installed in a QCM gas-sorption flow cell for further gas-sorption experiments.

Fig. 2 shows the optical microscope images and the corresponding gas adsorption and desorption graphs of the three states of the QCM. In the bare QCM electrode (Fig. 2(a)), the frequency decreased when SO_2 was introduced and then recovered when N_2 was introduced. This indicates that there was no adsorption of SO_2 on the bare QCM surface. For the MOF particles (Fig. 2(b)), the observed adsorption and desorption of SO_2 led to a distinctive sawtooth-shaped signal. This is attributed to the less uniform distribution and incomplete attachment of cobalt particles on the QCM surface, unlike in the case of the MOF film (Fig. 3(c)). These factors resulted in slight fluctuations

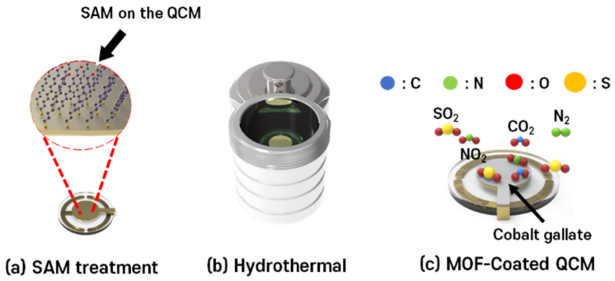

Fig. 1. Schematic of the fabrication of cobalt-gallate-coated QCM. (a) SAM treatment on the QCM, (b) hydrothermal process with the QCM electrode, and (c) gas flow adsorption of CO_2, NO_2, and SO_2 with cobalt-gallate-coated QCM.

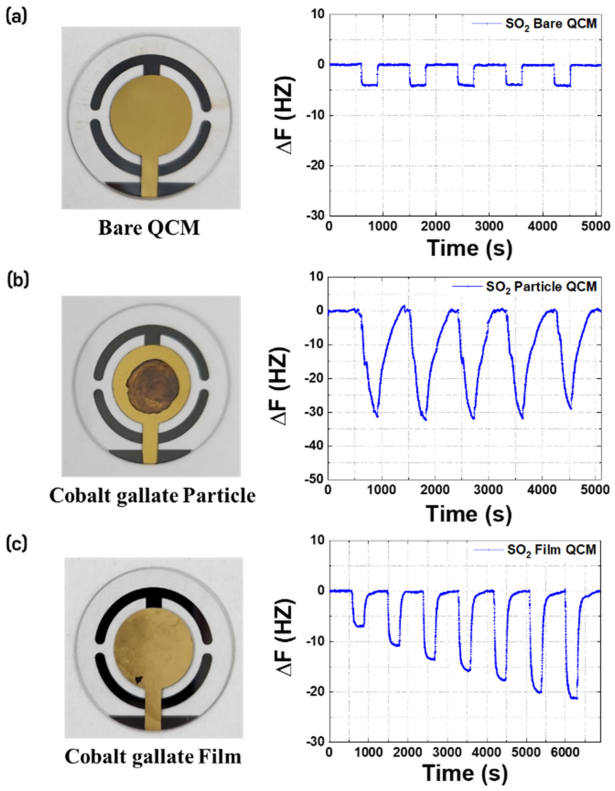

Fig. 2. Optical microscope images with SO_2 gas adsorption/desorption graphs with different states of QCMs. (a) Bare gold electrode QCM (b) cobalt gallate particles coated on the gold electrode of QCM. (c) cobalt gallate film was applied via SAMs on the gold electrode of QCM.

in the frequency change and delayed adsorption, preventing the achievement of a saturated frequency change. Consequently, the adsorption of SO_2 onto the MOF particles resulted in a distinct, sharp, sawtooth-shaped signal, which indicates a lower efficiency than that of the MOF film. In the MOF film (Fig. 3(c)), the change in the graph steadily increased as the concentration of SO_2 increased. This indicates that the MOF film was uniformly distributed on the QCM surface and that the adsorption of SO_2

was efficient.

Thus, as shown in Fig. 2, the cobalt gallate film outperformed the cobalt gallate particles in adsorbing SO_2, likely because of the uniform thickness and larger surface area of the film. The uniformity and increased surface area resulted in a more stable and efficient platform for SO_2 adsorption, suggesting the potential of cobalt gallate films for various SO_2 gas-detection applications. The film formation mechanism was also more discernible with a cobalt gallate film, which was achieved using the SAMs coating method [13].

In contrast, cobalt gallate particles showed greater instability and inefficiency in the adsorption process. This instability is reflected in the fluctuating frequency changes during adsorption and is further exacerbated by nonuniform particle deposition on the QCM gold electrode. This uneven deposition negatively affects the stability of the particle coating in the QCM system designed to measure mass changes with nanogram precision [14].

As shown in Fig. 3(a) and 3(b), SAMs 1-dodecanethiol (12-CH_3) and 1-octanethiol (8-CH_3), which terminate in the methyl groups, displayed the contact angles of 105.3 ° and 99.2 °, respectively, indicating hydrophobic properties. Conversely, Fig. 3(c) and 3(d) illustrate the SAMs 11-mercaptoundecanoic acid (11-COOH) and 11-mercaptoundecanol (11-OH), respectively, which contain carboxylate and hydroxyl groups. These SAMs showed smaller contact angles of 30.1 ° and 17.1 °, respectively, indicating hydrophilic characteristics.

Unlike 12-CH_3 and 8-CH_3, shown in Fig. 3(a) and 3(b), respectively, which possess nonpolar functional groups (methyl groups), 11-COOH in Fig. 3(c) and 11-OH in Fig. 3(d) both have polar functional groups (carboxylate and hydroxyl groups). These polar groups contain positively and negatively charged regions, enabling them to form hydrogen bonds with water droplets. This interaction reduces the surface energy and improves surface wettability, resulting in hydrophilic contact angles [15, 16]. Consequently, hydrogen bonding also contributes to a lower contact angle for the hydroxyl (OH) group than for the carboxyl (COOH) group, as depicted in Fig. 3(c) and 3(d). This is because the hydroxyl group has a higher propensity to form hydrogen bonds with water molecules, thereby exhibiting greater hydrophilicity.

The cobalt gallate coating was less effective in Fig. 4(a) and 4(b) than in Fig. 4(c) and 4(d) owing to the variation in the SAM types used in the coating [17]. In the functional groups in Fig. 4(a) and 4(b), the molecules ending in CH_3 are nonpolar, making them less receptive to binding with the metal ions and the OH groups of gallic acid. In contrast, the functional groups shown in Fig. 4(c) and 4(d), COOH and OH, are polar and partially charged, facilitating their binding to the metal ions and the OH groups of gallic acid. Specifically, the COOH SAM, as depicted in Fig. 4(c), exhibited the largest coating amount. This outcome is attributed to the more polar COOH, which has a larger charge dispersion and higher charge density than OH [18]. In the water contact angle experiment shown in Fig. 3, COOH displayed a higher contact angle, indicating a lower affinity for water. However, the hydrophilicity and binding of metal ions to gallic acid are distinct issues, and it is inferred that a higher charge density plays a more critical role in achieving an efficient cobalt gallate coating.

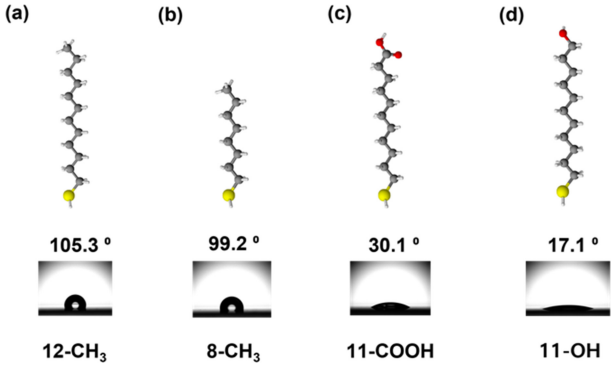

Fig. 3. Chemical structure of SAMs and contact angle on the QCM gold electrode. (a) CH_3 functional group 1-dodecanethiol (12-CH_3), (b) 1-octanethiol (8-CH_3), COOH functional group (c) 11-mercaptoundecanoic acid (11-COOH), OH functional group (d) 11-mercaptoundecanol (11-OH), (gray–carbon, white–hydrogen, red–oxygen, yellow–sulfur) (The number in front indicates the number of carbons, and the notation that follows indicates the functional group).

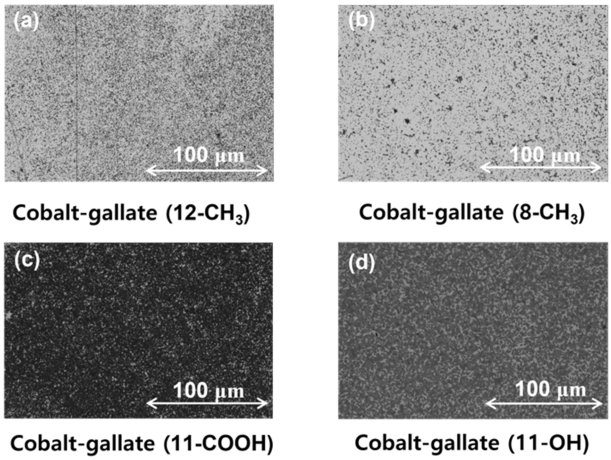

Fig. 4. Optical microscope images of cobalt gallate on a gold surface corresponding to the SAMs in Fig. 3 (The black region represents cobalt gallate, whereas the white region represents the gold surface).

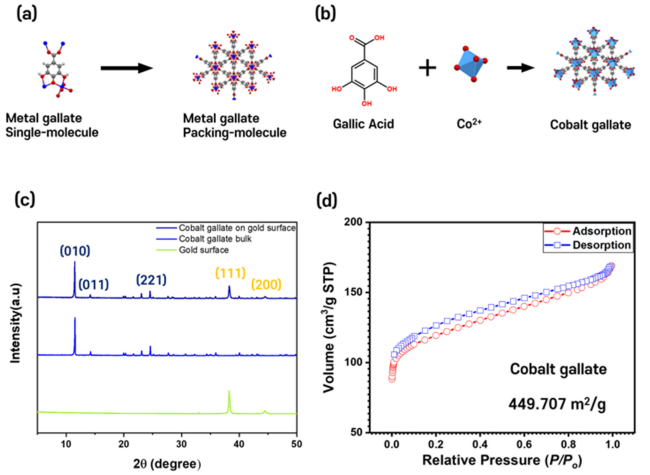

Fig. 5. (a) Molecular structure of cobalt gallate drawn using Mercury CCDC, (b) synthesis of cobalt gallate drawn using Diamond 4, (c) multipurpose XRD patterns of cobalt gallate film and gold surface, and (d) surface area of cobalt gallate determined by BET.

3.2 Characterization of Cobalt gallate film on QCM

The single molecular and packing structures of cobalt gallate are depicted in Fig. 5(a), as visualized using Mercury CCDC. The synthesis of metal gallate as a packing molecule is illustrated in Fig. 5(b), created using Diamond 4. These images illustrate the simple synthesis of the cobalt gallate MOF.

The XRD patterns of cobalt gallate are shown in Fig. 5(c). The XRD pattern of the cobalt gallate particles reveals main peaks at (010), (011), and (221), corresponding to the diffraction angles of 11.66 °, 14.34 °, and 24.83 °, respectively. These peaks match the reference values [19]. In the XRD pattern of the gold surface, the main peaks were observed at (111) and (200) at the specific angles of 38.25 ° and 44.44 °, respectively [20]. When the cobalt gallate film was deposited on the gold surface, the XRD pattern exhibited peaks identical to those observed for both the cobalt gallate film and gold surface.

As shown in Fig. 5(d), the BET measurement for cobalt gallate indicated a large surface area of 449.7 m^2/g. This value aligns with the reference data from previous experiments [21]. In addition, cobalt gallate has a pore size of 0.260 cm^3/g.

The FESEM images of the cobalt gallate film deposited on the gold surfaces are presented in Fig. 6. Fig. 6(a) shows the top view of the densely deposited cobalt gallate film covering the gold substrate entirely. The average size of a single cobalt gallate particle is 639 ± 86 nm. The cross-sectional view shown in Fig. 6(b) reveals an average thickness of 2.171 ± 0.939 μm for the cobalt gallate film.

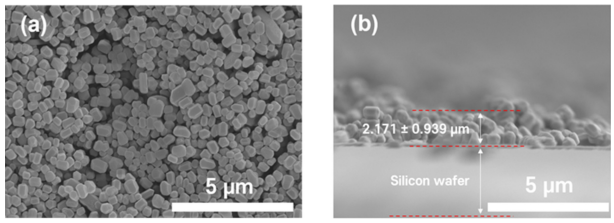

Fig. 6. FESEM images of the cobalt gallate film on the gold surface. (a) Top view and (b) cross-section.

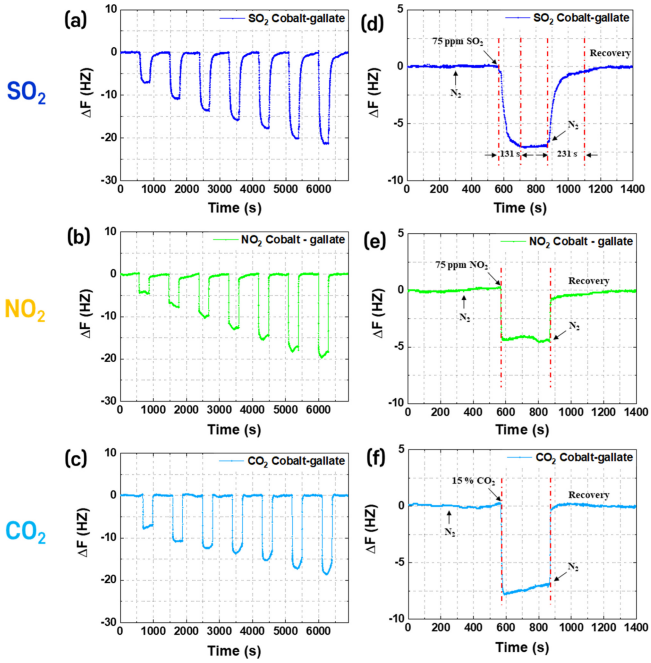

Fig. 7. (a–c) Graphs of the adsorption and desorption of SO_2, NO_2, and CO_2 gases on the cobalt-gallate-coated QCM film. The concentrations of SO_2 and NO_2 gases are sequentially increased at 75, 150, 225, 300, 375, 450, and 500 ppm, and (c) shows the adsorption and desorption of CO_2 gas at the concentrations of 15 %, 30 %, 45 %, 60 %, 75 %, 90 %, and 100 %. (All gas injections were performed in N_2: 300 s; SO_2, NO_2, and CO_2: 600 s.) (d–f) are magnified graphs of the initial adsorption and desorption of SO_2, NO_2, and CO_2, respectively.

3.3 Gas Adsorption & Desorption Property of Cobalt Gallate Film

To quantify gas adsorption on the QCM surface, the mass change was proportional to the change in the QCM frequency according to the Sauerbrey equation. By comparing the graphs in Fig. 7(a–c), it is observed that SO_2 and NO_2 adsorption occurred even at a low concentration of 75 ppm, whereas CO_2 adsorption

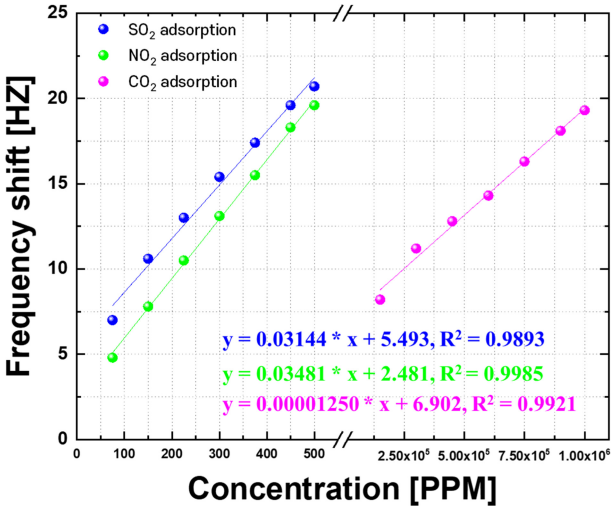

Fig. 8. Frequency shifts for different concentrations of SO_2 (blue line), NO_2 (green line), and CO_2 (magenta line).

occurred at a high concentration of 15 %, with similar frequency changes. Therefore, the synthesized cobalt gallate film was highly selective for the gaseous particulate matter of SO_2 and NO_2 compared with CO_2.

By analyzing the adsorption-desorption mechanism of cobalt gallate from Fig. 7(d–f), it was observed that the SO_2 adsorption-desorption delays were 131 and 231 s for adsorption and desorption, respectively. In contrast, no adsorption-desorption delay was observed for NO_2 and CO_2, suggesting that cobalt gallate particularly interacts with SO_2 gas. Cobalt gallate exhibited a larger amount of adsorption of SO_2 than NO_2. The adsorption and desorption rates of SO_2 gas were lower than those of NO_2 and CO_2, but the amount of SO_2 adsorbed was the largest relative to the concentration of the gases. Therefore, cobalt gallate has high selectivity for SO_2 and a considerable adsorption capacity.

Fig. 8 shows the fitting results for the adsorption amounts according to the concentrations of SO_2, NO_2, and CO_2. Cobalt gallate exhibited much higher vibrational frequency changes at the same concentration levels for SO_2 and NO_2 than for CO_2. Additionally, cobalt gallate showed a smaller adsorption capacity for CO_2, and as shown in Fig. 7, there was no interaction between cobalt gallate, and CO_2 gas. Therefore, cobalt gallate has a higher selectivity for SO_2 and NO_2 than for CO_2. Moreover, it has the highest selectivity for SO_2, as it shows a larger adsorption amount than that for NO_2 at the same concentration level.

The limit of detection (LOD) of the cobalt gallate film on the QCM was evaluated. The cobalt gallate film was unable to detect low concentrations of CO_2 but could detect SO_2 and NO_2 at low concentrations. To determine the LOD for SO_2, NO_2, and CO_2, calibration curves ($y = 0.03144x + 5.493$, $R^2 = 0.9893$; $y = 0.03481x + 2.481$, $R^2 = 0.9985$; $y = 0.00001250x + 6.902$, $R^2 = 0.9921$) were generated using the data from Fig. 8 and Equation (2) [22].

$$LOD = \frac{3\sigma}{S} \tag{2}$$

σ is the standard deviation of the response (0.56, 0.23, 0.38), and S is the slope of the calibration curve (0.03144, 0.3481, 0.00001250). These parameters were used to determine the logical detection limits of the cobalt gallate film on the QCM for SO_2, NO_2, and CO_2, which were observed to be 53.44, 19.92, and 91797.97 ppm, respectively. The developed sensor can detect and quantify gaseous particulate matter adsorption in real time using the QCM. Although the sensitivity of the sensor was higher than the concentrations that affect human health, further experiments are required to establish its true sensitivity within a lower concentration range. This study lays the groundwork for developing sensors with high sensitivity and selectivity for gaseous particulate detection.

4. CONCLUSIONS

In this study, we demonstrated the potential of cobalt-gallate-based MOF films for gas-sensing applications using the QCM technique. The cobalt gallate film deposited on the QCM exhibited high efficiency and stability in adsorbing SO_2, making it a promising material for various SO_2 gas-detection applications. This study highlighted the importance of functional groups with polar molecules in facilitating an efficient cobalt gallate coating. The cobalt gallate film was highly selective for the gaseous particulate matter of SO_2 and NO_2 compared with CO_2, suggesting its potential for developing MOF-based sensors for detecting NO_2 and SO_2 gases with enhanced performance and selectivity. This study clarified the adsorption mechanism of cobalt gallate and can potentially drive the development of MOF-based sensors for air-quality monitoring.

ACKNOWLEDGMENT

This study was supported by the National Research Foundation of Korea (NRF) grant funded by the Korean Government (MSIT) (No. NRF-2021R1A5A8033165).

REFERENCES

[1] S. Lee and H. W. Jang, "α-Fe2O3 nanostructure-based gas sensors", *J. Sens. Sci. Technol.*, Vol. 30, No. 4, pp. 210–217, 2021.

[2] J. F. Chan, J. K. Jeon, Y. K. Moon, and J. H. Lee, "Highly sensitive xylene sensors using Fe2O3-ZnFe2O4 composite spheres", *J. Sens. Sci. Technol.*, Vol. 30, No. 4, pp. 191–195, 2021.

[3] J. W. Jung and J. S. Jang, "Nanocatalyst Decorated Metal Oxides on Highly Selective Chemical Sensors", *J. Sens. Sci. Technol.*, Vol. 31, No. 4, pp. 187–193, 2022.

[4] S. Woo, "Metal-organic frameworks-driven ZnO-functionalized carbon nanotube fiber for NO2 sensor", *J. Sens. Sci. Technol.*, Vol. 30, No. 6, pp. 369–375, 2021.

[5] L. Wang, "Metal-organic frameworks for QCM-based gas sensors: A review", *Sens. Actuators Phys.*, Vol. 307, p. 111984, 2020.

[6] I. R. Jang and H. J. Kim, "Short Review on Quartz Crystal Microbalance Sensors for Physical, Chemical, and Biological Applications", *J. Sens. Sci. Technol.*, Vol. 31, No. 6, pp. 389–396, 2022.

[7] Y. Kim, "Highly sensitive and selective NO2 gas sensor at low temperature based on SnO2 nanowire network", *J. Sens. Sci. Technol.*, Vol. 30, No. 3, pp. 175–180, 2021.

[8] S. Y. Bak, S. H. Lee, C. Y. Park, D. Baek, and M. Yi, "Study on the Performance Improvement of ZnO-based NO2 Gas Sensor through MgZnO and MgO", *J. Sens. Sci. Technol.*, Vol. 31, No. 6, pp. 455–460, 2022.

[9] M. J. Hwang, W. G. Shim, and H. Moon "A QCM-based Sensor System for Detecting NO_2 and SO_2", *Korean Chem. Eng. Res.*, Vol. 51, No. 2, pp. 285–291, 2013.

[10] J. C. Love, L. A. Estroff, J. K. Kriebel, R. G. Nuzzo, and G. M. Whitesides, "Self-Assembled Monolayers of Thiolates on Metals as a Form of Nanotechnology", *Chem. Rev.*, Vol. 105, No. 4, pp. 1103–1170, 2005.

[11] F. Chen, "Deep Desulfurization with Record SO_2 Adsorption on the Metal–Organic Frameworks", *J. Am. Chem. Soc.*, Vol. 143, No. 24, pp. 9040–9047, 2021.

[12] C. Yim, M. Yun, N. Jung, and S. Jeon, "Quartz Resonator for Simultaneously Measuring Changes in the Mass and Electrical Resistance of a Polyaniline Film", *Anal. Chem.*, Vol. 84, No. 19, pp. 8179–8183, 2012.

[13] P. Falcaro, R. Ricco, C. M. Doherty, K. Liang, A. J. Hill, and M. J. Styles, "MOF positioning technology and device fabrication", *Chem Soc Rev.*, Vol. 43, No. 16, pp. 5513–5560, 2014.

[14] V. Stavila, J. Volponi, A. M. Katzenmeyer, M. C. Dixon, and M. D. Allendorf, "Kinetics and mechanism of metal–organic framework thin film growth: systematic investigation of HKUST-1 deposition on QCM electrodes", *Chem. Sci.*, Vol. 3, No. 5, p. 1531, 2012.

[15] D. Mao, X. Wang, Y. Wu, Z. Gu, C. Wang, and Y. Tu, "Unexpected hydrophobicity on self-assembled monolayers terminated with two hydrophilic hydroxyl groups", *Nanoscale*, Vol. 13, No. 46, pp. 19604–19609, 2021.

[16] C. Zhu, "Characterizing hydrophobicity of amino acid side chains in a protein environment via measuring contact angle of a water nanodroplet on planar peptide network", *Proc. Natl. Acad. Sci.*, Vol. 113, No. 46, pp. 12946–12951, 2016.

[17] O. Shekhah, J. Liu, R. A. Fischer, and Ch. Wöll, "MOF thin films: existing and future applications", *Chem. Soc. Rev.*, Vol. 40, No. 2, p. 1081, 2011.

[18] J. DeRuiter, "Carboxylic Acid Structure and Chemistry Part 1", *in Principle of Drug Action 1*, *Auburn University, Alabama*, pp. 1-11, 2005.

[19] G. Chen, X. Chen, Y. Pan, Y. Ji, G. Liu, and W. Jin, "M-gallate MOF/6FDA-polyimide mixed-matrix membranes for C2H4/C2H6 separation", *J. Membr. Sci.*, Vol. 620, p. 118852, 2021.

[20] J. Hu, X. Huang, S. Xue, G. Yesilbas, A. Knoll, and O. Schneider, "Measurement of the mass sensitivity of QCM with ring electrodes using electrodeposition", *Electrochem. Commun.*, Vol. 116, p. 106744, 2020.

[21] B. Liang, "An Ultramicroporous Metal–Organic Framework for High Sieving Separation of Propylene from Propane", *J. Am. Chem. Soc.*, Vol. 142, No. 41, pp. 17795–17801, 2020.

[22] Z. Ma, "A benzene vapor sensor based on a metal-organic framework-modified quartz crystal microbalance", *Sens. Actuators B Chem.*, Vol. 311, p. 127365, 2020.